***Oncogene***

# Autocrine HGF/c-Met signaling pathway confers aggressiveness in lymph node adult T-cell leukemia/lymphoma

Running title: Roles of HGF/c-Met in ATL

Haruhito Totani[1, 2], Keiko Shinjo[1], Miho Suzuki[1], Keisuke Katsushima[1], Shoko Mase[1], Ayako Masaki[2, 3], Asahi Ito[2], Masaki Ri[2, 4], Shigeru Kusumoto[2], Hirokazu Komatsu[2], Takashi Ishida[5], Hiroshi Inagaki[3], Shinsuke Iida[2], and Yutaka Kondo[1]*.

1. Division of Cancer Biology, Nagoya University Graduate School of Medicine, Nagoya, Japan
2. Department of Hematology and Oncology, Nagoya City University Graduate School of Medical Sciences, Nagoya, Japan
3. Department of Pathology and Molecular Diagnostics, Nagoya City University Graduate School of Medical Sciences, Nagoya, Japan
4. Department of Blood Transfusion and Cell Therapy, Nagoya City University Hospital, Nagoya, Japan
5. Department of Immunology, Nagoya University Graduate School of Medicine, Nagoya, Japan

**Conflict of interest:** The authors disclose no potential conflicts of interest.

*Correspondence to:

Yutaka Kondo, MD, PhD
Division of Cancer Biology
Nagoya University Graduate School of Medicine
65 Tsurumai-cho, Showa-ku,
Nagoya 466-8550, Japan
TEL: +81-52-744-2463
FAX：+81-52-744-2464
E-mail: ykondo@med.nagoya-u.ac.jp

**Abstract**

Adult T-cell leukemia/lymphoma (ATL) is an aggressive T-cell neoplasm. While ATL cells in peripheral blood (PB-ATL) are sensitive to anti-CC chemokine receptor 4 treatment, non–PB-ATLs, including lymph node ATLs (LN-ATLs), are more aggressive and resistant. We examined characteristic cytokines and growth factors that allow non–PB-ATLs to proliferate and invade compared to PB-ATLs. Protein array analysis revealed hepatocyte growth factor (HGF) and C-C motif chemokine 2 (CCL2) were significantly upregulated in non–PB-ATLs compared to PB-ATLs. The HGF membrane receptor, c-Met, was expressed in PB-ATL and non–PB-ATL cell lines, but CCR2, a CCL2 receptor, was not. Immunohistochemical analysis in clinical ATLs revealed high HGF expression in LNs, pharynx, bone marrow, and tonsils. The HGF/c-Met signaling pathway was active downstream in non–PB-ATLs. Downregulation of HGF/c-Met by siRNA or chemical inhibitors decreased *in vitro* and *in vivo* proliferation and invasion by non–PB-ATLs. Treatment with bromodomain and extra-terminal motif inhibitor suppressed HGF expression and decreased levels of histone H3 lysine 27 acetylation (H3K27Ac) and bromodomain-containing protein 4 (BRD4) binding promoter and enhancer regions, suppressing non–PB-ATL cellular growth. Our data indicate H3K27Ac/BRD4 epigenetics regulates the HGF/c-MET pathway in ATLs; targeting this pathway may improve treatment of aggressive non–PB-ATLs.

**Keywords**: Hepatocyte growth factor, Epigenetic regulation, Adult T-cell leukemia/lymphoma

## Introduction

Adult T-cell leukemia lymphoma (ATL) is a peripheral T-cell lymphoma caused by human T-cell leukemia virus type I (HTLV-1)[1-3]. ATL is classified into four types: acute, lymphoma, chronic, and smoldering, depending on clinical features such as morphology, the number of abnormal lymphocytes in the peripheral blood (PB), lactate dehydrogenase level, calcium level, and ATL lesions [4]. Of these, acute, lymphoma, and unfavorable chronic types have a poor prognosis due to their aggressiveness, invasiveness, and resistance to treatments [5]. At diagnosis, more than 90% of such aggressive ATLs already have non-PB lesions, such as lymph node, liver, bone marrow, and skin infiltrations, which are the most frequent lesions [1, 6-8].

Recently, mogamulizumab, a newly developed anti-CC chemokine receptor 4 (CCR4) monoclonal antibody, became an effective therapeutic option for ATL, being particularly effective in improving outcomes for PB lesions [9, 10]. Responses in non-PB lesions are less effective than PB lesions: response rates are 100%, 25–92%, and 63–75% in PB, nodal and extranodal, and skin lesions, respectively. In addition, although clinical remission was reached by mogamulizumab, a set of cases with non-PB lesions experienced relapse [11]. Therefore, the presence of non-PB lesions in patients with ATL appears detrimental in a prognosis.

Although monoclonal proliferation of ATL is expected during early tumorigenesis, acute-type ATL has multiple subclones that originate as a result of the clonal expansion of ATL cells. Indeed, comprehensive genome analysis revealed that the genomic alteration profiles of lymph node (LN) lesions differed to those of PB lesions [12]. Recent studies have shown that epigenetic dysregulation is involved during the progression of ATL [13-16]. Given the dynamic effects of epigenetic mechanisms on cancer cells, the multiple subclones/heterogeneity found in ATLs may also occur through epigenetic mechanisms.

Cytokines and growth factors have been known to affect not only tumor cell behavior but also

the formation of the tumor microenvironment. Hepatocyte growth factor (HGF) and the c-Met receptor (HGF/c-Met) signaling pathway are known to promote tumor proliferation, invasion, and metastasis in many types of cancers [17-19]). This pathway is also associated with aggressive ATL. Increased expression of c-Met in ATL cells as well as increased HGF in plasma have been detected in a set of patients with aggressive acute ATLs, although the underlying mechanism for increased plasma levels of HGF in ATL patients is mostly unclear [20-22].

In the current study, we examined characteristic cytokine and growth factor signaling pathways in non–PB-ATLs, which confer ATL cells with more proliferative and invasive features in comparison to PB-ATLs. We found that expression levels of HGF in ATL cells differ according to their lesion location via dynamic epigenetic mechanisms in each patient. Further, the bromodomain and extra-terminal motif (BET) inhibitor, JQ1, effectively repressed HGF expression together with inhibition of tumorigenesis and invasiveness in ATL, both *in vitro* and *in vivo*. Our data indicate that targeting the HGF/c-Met axis may be a novel and efficient therapeutic for patients with non–PB-ATL.

## Results

### *High expression of HGF in both LN-ATL cell lines and clinical samples*

To identify highly expressed cytokines and growth factors in non–PB-ATL rather than PB-ATL, cytokine and growth factor protein array was performed in non–PB-ATL (e.g. LN-ATL; HUT102) and PB-ATL (MT-1, TL-Om1, and ATN-1) cell lines. Of 80 proteins, the expression levels of HGF and C-C motif chemokine 2 (CCL2) were significantly increased in LN-ATL compared to PB-ATL cell lines (Fig. 1A). High expression of HGF and CCL2 in LN-ATL cell lines was validated by Enzyme-Linked Immunosorbent Assay (ELISA) (Fig. 1B). Messenger RNA

expression of *HGF* and *CCL2* was also high in the LN-ATL cell line, while these were substantially lower in PB-ATL cells and non-ATL cell lines (TL-Su and $CD4^+$ T-cell; Fig. 1C). *c-Met*, which encodes the HGF receptor, was expressed in all ATL cell lines examined regardless of their original tumor location, while the CCL2 receptor, *CCR2*, was not expressed in all ATL cell lines. These data indicate that HGF may act in an autocrine manner to activate the c-Met pathway in LN-ATLs.

Next, we examined HGF expression in 15 clinical ATL cases with non-PB lesions (lymph node, pharynx, tonsil, bone marrow, and tongue). We found that 11 cases showed moderate to high HGF expression in ATL cells in non-PB lesions, such as in the LN, pharynx, tongue, and tonsils (Fig. 1D, Table 1). Samples from both PB and non-PB lesions were available in seven ATL cases. Of these, non-PB ATL cells showed a relatively higher expression of HGF compared to PB-ATL cells in four cases, although a subset of PB-ATL cells were also HGF positive. A gradual increase in HGF-positive cells from PB to non-PB indicates that HGF expression may foster tumor growth in non-PB tissues.

***HGF promotes ATL proliferation and invasion***

Cell proliferation was significantly promoted by exogenous HGF stimulation in both MT-1 and TL-Om1 cells (PB-ATL, $P < 0.01$, Fig. 2A). Similarly, HGF overexpression promoted cell proliferation in both MT-1 and TL-Om1 cells ($P < 0.01$, Fig. 2B). By contrast, HGF suppression by short hairpin (sh)RNA led to slower cell growth in non–PB-ATL HUT102 cells (Fig. 2C). A cell invasion assay revealed that both overexpressed and exogenous HGF induced ATL cell invasion in MT-1 and TL-Om1 cells ($P < 0.01$, Fig. 2D, E).

Further, we examined the effects of HGF on ATL cells *in vivo*. NOD/Shi-scid, IL-2RγKO (NOG) mice with intraperitoneally transplanted TL-Om1 cells with HGF expression formed

tumor masses in the abdominal cavity and showed marked abdominal distension and splenomegaly. In contrast, mice injected with TL-Om1 cells with a control vehicle vector showed no obvious tumor formation (Fig. 2F). The weights of tumor masses, liver, ascites, and spleens, and the surface area of spleens, were all significantly larger in mice of the TL-Om1 with HGF expression group compared to those of the control TL-Om1 group ($P < 0.01$, Fig. 2G). Immunohistochemical analysis showed that in mice in the TL-Om1 with HGF expression group, ATL cells were scattered and had infiltrated around blood vessels, such as the portal vein in the liver, and also diffusely infiltrated the spleen. Furthermore, tumor masses of ATL cells were observed on the surface of livers and spleens (Fig. 2H, Supplementary Fig. S1A, S1B).

***HGF/c-Met signaling and its activation***

Since HGF/c-Met signals are continuously activated in HUT102 cells, further stimulation by HGF did not significantly alter downstream signals (Fig. 3A). By contrast, both exogenous HGF stimulation and HGF overexpression significantly activated the HGF/c-Met signaling pathway in MT-1 and TL-Om1 cells ($P < 0.01$, Fig. 3A, 3B). Intriguingly, protein levels of c-Met were almost at a baseline level in contrast to the high level of *c-Met* mRNA in HUT102 cells, indicating the post-transcriptional regulation of c-Met expression (Fig. 1C). Inhibition of proteasome and V-ATPase by MG132 and concanamycin A, which inhibit ubiquitination and internalization, respectively, led to the recovery of c-Met protein expression, indicating that continuous HGF exposure induces the internalization of c-Met in HUT102 cells. The internalization of c-Met was also observed after continuous exposure to HGF in MT-1 and ATN-1 cells (Supplementary Fig. S2A, S2B).

In HUT102 cells, c-Met phosphorylation and downstream Akt phosphorylation were efficiently inhibited by a c-Met ATP-competitive kinase inhibitor, PHA-665752, in a dose-

dependent manner (Fig. 3C). PHA-665752 treatment effectively induced the growth suppression of HUT102 cells, which was partially rescued by additional HGF stimulation, indicating that activation of HGF/c-Met and its downstream pathways contributes, at least in part, to the proliferation of such cells (Fig. 3D, E).

***Regulation of HGF expression by epigenetic mechanisms***

Given that the HGF expression level was heterogeneous and appeared to be associated with locations of major lesions of ATL cells in a patient, epigenetic mechanisms may be involved in the dynamic regulation of HGF expression. Gene regulatory regions of the *HGF* gene, including an enhancer (E) and a promoter (P), were identified using a public chromatin immunoprecipitation (ChIP)–Atlas database (https://chip-atlas.org/)[23](Fig. 4A, Supplementary Fig. S3A). We examined the enrichment of the acetylation of histone H3 lysine 27 (H3K27Ac) and its binding protein, bromodomain-containing protein 4 (BRD4) in the regulatory regions of the *HGF* gene. ChIP–PCR analysis revealed that both H3K27Ac and BRD4 were enriched in the enhancer and promoter regions of *HGF* in HUT102 cells, with baseline enrichment levels of both H3K27Ac and BRD4 in TL-Om1 cells. Notably, treatment with a bromodomain inhibitor, JQ1, decreased BRD4 enrichment and H3K27Ac in HUT102 cells, which resulted in the significant suppression of HGF expression and HGF/c-Met pathway activity (Fig. 4B, 4C, and 4D). JQ1 treatment also induced significant suppression of cell proliferation in HUT102. This growth suppression was partially rescued by HGF overexpression or exogenous HGF treatment ($P < 0.01$, Fig. 4E, Supplementary Fig S3B). We further documented that the induction of apoptosis in HUT102 by JQ1 treatment was rescued by caspase inhibitors. Thus, JQ1-induced apoptosis is involved in suppression of cell proliferation (Fig. 4F, G).

***Suppression of ATL invasion by JQ1 treatment***

To clarify the effects of JQ1 *in vivo*, HUT102 cells were intraperitoneally transplanted into NOG mice, followed by JQ1 treatment after seven days of transplantation (Fig. 4H). In the control group, ascites, enlargement of the spleen and liver, and the formation of multiple tumors in the abdominal cavity were observed, whereas almost no ascites or enlargement of the spleen and liver, but a limited number of tumors, were detected in the JQ1 treatment group (Fig. 4I). The weights of liver, spleen, and ascites showed marked decreases in the JQ1 treatment group in comparison with the control group ($P < 0.01$, Fig. 4J). Consistently, histological findings showed marked antitumor effects in the JQ1 treatment group (Fig. 4K). Taken together, HGF expression was regulated by an epigenetic mechanism, which was effectively inhibited by JQ1 bromodomain inhibitor, resulting in the suppression of ATL cell growth and its invasive activity into organs such as the liver, spleen, and abdomen.

***HGF expression in clinical samples***

High levels of HGF were reported in the plasma of patients with acute type ATL [20]. HGF expression in sera was compared between patients with aggressive ATL (acute and lymphoma types) and healthy individuals. In both patients with acute and lymphoma type ATL, HGF levels were significantly higher than in patients of the control group ($P < 0.05$), although a significant difference was not apparent between ATL types (Fig. 5A). Notably, patients with aggressive ATL and non-PB showed significantly higher levels of serum HGF compared to patients with ATL without non-PB lesions ($P < 0.05$, Fig. 5B).

Interestingly, for 26 patients with ATL who received mogamulizumab treatment, median progression-free survival (PFS) was 420 and 116 days, and median overall survival (OS) was 704 and 344 days, in low and high HGF groups, respectively ($P < 0.05$; OS, $P < 0.05$; Fig. 5C). Taken

together, patients with aggressive ATL and non-PB showed a high level of HGF in serum, leading to a poor outcome after mogamulizumab treatment.

**Discussion**

Increased expression of c-Met in ATL cells as well as increased plasma HGF have been detected in some patients with aggressive acute ATLs, although the underlying mechanism is not very clear [20-22]. In the current study, we showed that upregulated HGF/c-Met signaling in non–PB-ATL confers proliferative and invasive properties on ATL cells; this may be associated with the aggressiveness of ATL and responsiveness to mogamulizumab treatment. In particular, an HGF-dependent autocrine c-Met activation mechanism was considered to effectively support tumors growing in non–PB-ATL lesions, such as in LNs. Given the existence of a heterogeneous population in ATLs, each tumor cell with a different gene expression status shows a different characteristic behavior [24]. A previous analysis using array-based comparative genomic hybridization (CGH) demonstrated that multiple subclones in LNs originate from a common clone and that selected subclones appeared in the PB after subclones developed in LNs [12]. We further demonstrated here that an epigenetic mechanism confers heterogeneity in ATL tissues. Although ATL cells in non-PB showed substantially higher expression of HGF in comparison with ATL cells in PB, a proportion of the latter also show moderately elevated HGF expression. Regarding the aforementioned CGH analysis, it is possible that PB clones may appear after subclones with high HGF expression had developed in LNs.

Recent studies have shown that epigenetic mechanisms are involved in the progression of ATL [13-16]. Indeed, as a clinical practice, epigenetic approaches to T-cell lymphomas in systemic and/or local infiltrating tissues have been undertaken, such as the use of histone deacetylase inhibitors (e.g. romidepsin and vorinostat) for peripheral T-cell lymphoma and cutaneous T-cell

lymphoma [25-27]. In the current study, we identified that the displacement of BRD4 from H3K27 enriched enhancer and promoter chromatin while JQ1 efficiently reduced HGF expression. Consistent with our data, a previous study demonstrated that JQ1 treatment reduced basic leucine zipper ATF-Like transcription factor 3 (BATF3) mRNA and protein levels in ATLs, which correlated with the eviction of BRD4 from a BATF3 super-enhancer. Depletion of BATF3 in ATL cells by JQ1 treatment effectively inhibited the growth of ATL cells, both *in vitro* and *in vivo*, together with leading to a decreased level of MYC [28]. These multiple effects in JQ1 data may explain why HGF overexpression only partially rescued tumor cell growth in response to JQ1 treatment. However, JQ1 reduced HGF expression, which resulted in the subsequent inactivation of downstream Akt and MAPK pathways, thereby suppressing cell growth in the current study. In other words, the partial effects of HGF after JQ1 treatment indicates that although HGF/c-Met is one of the important signaling pathways for ATL progression, targeting HGF/c-Met alone is not sufficient for the treatment of aggressive ATLs.

Our data demonstrated that the high HGF group showed a worse prognosis compared to the low HGF group after treatment with mogamulizumab, indicating that the presence of HGF-producing ATL cells in non-PB lesions may be a predictive marker for a treatment response. Consistently, studies showed that expression levels of c-Met in ATL cells and those of HGF in plasma are increased in patients with aggressive ATL, although the precise underlying mechanism for the aggressive behavior of ATL was mostly unclear [20-22]. Mogamulizumab induced antibody-dependent cellular cytotoxicity by NK cells against CCR4-positive cells. Previous studies have shown that HGF promotes monocyte differentiation toward tolerogenic dendritic cells together with the substantial expression of indoleamine 2,3-dioxygenase 1 (IDO), which effectively suppresses the activity of T and NK cells [29, 30]. Indeed, high IDO activity in sera predicts poor prognosis in ATL patients [31]. Therefore, in addition to increasing cell proliferation

and invasion, increased HGF in non-PB lesions may affect the immune system in the ATL tumor microenvironment.

An earlier study had shown that HGF inhibited chemotherapy-induced apoptosis by protecting the anti-apoptotic proteins Bcl-XL and Bcl-2 [32]. Our data showed that JQ1 treatment effectively induced apoptosis, which could be at least partially explained by the downregulation of HGF/c-Met signaling by JQ1. Although further study is required, BET inhibitors might be a potential treatment option for a patient who is mogamulizumab and/or chemotherapy resistant.

In conclusion, we demonstrated here that HGF expression was upregulated via an epigenetic mechanism in non-PB lesions of patients with ATL, which results in the formation of ATL tumors, and may be associated with mogamulizumab resistance. Our data provides evidence that a BET inhibitor, which showed substantial antitumor effects against non-PB ATLs, may be a new therapeutic approach for aggressive ATL with non-PB lesions.

## Materials and Methods

### *ATL samples and cell lines*

Samples from 57 ATL patients and 10 healthy non-leukemic patients were obtained at Nagoya City University Hospital, Japan, between January 2007 and December 2019. All samples were collected with written informed consent after approval by the Institutional Ethics Committees of Nagoya City University (No. 70-00-0113). Peripheral blood mononuclear cells (PBMCs) were isolated using Ficoll-Paque PLUS (GE Healthcare Life Sciences, Buckinghamshire, UK). Normal $CD4^+$ lymphocytes were separated from PBMCs using anti-human CD4 microbeads (130-045-101, Miltenyi Biotec GmbH, Bergisch Gladbach, Germany). For serum, collected whole blood was allowed to stand for 30 min at room temperature, and then the clot was removed by

centrifuging at 1,000×g for 10 min at 4°C. The ATL cell lines, MT-1, TL-Om1, and ATN-1, were originally established from PB-ATL cells, and HUT102 was established from a LN (LN-ATLs). TL-Su is an HTLV-1 immortalized cell line established from HTLV-1 carrier blood, as previously described [2, 33-36]. MT-1 was obtained from the Japanese Collection of Research Biosources Cell Bank (National Institute of Biomedical Innovation, Osaka, Japan). ATN-1 was obtained from the RIKEN BioResource Center (Tsukuba, Japan). HUT102 was obtained from the American Type Culture Collection (Manassas, VA, USA). These cell lines were authenticated through short tandem repeat profiling by the JCRB Cell Bank and tested and found to be mycoplasma free. TL-Om1 and TL-Su were provided by the Cell Resource Center for Biomedical Research (Tohoku University, Sendai, Japan). Although these cell lines were not authenticated, cells at a relatively low passage number were obtained. Cell lines were maintained in RPMI-1640 medium (Wako, Osaka, Japan) containing 10% fetal bovine serum (Thermo Fisher Scientific, Waltham, MA, USA) and 1% penicillin–streptomycin (Wako) at 37°C in a humidified incubator with 5% $CO_2$.

***Plasmid construction, lentivirus production and establishment of stable cell lines***

The *HGF* gene was amplified by PCR using KOD-plus-neo (Toyobo, Osaka, Japan). The primer sequences are shown in Supplementary Table S1. The amplified DNA fragment was inserted into a pENTR/D-TOPO vector (Thermo Fisher Scientific), followed by transfer into a CSII-CMV-RfA-IRES2-Venus vector plasmid using Gateway cloning technology (Thermo Fisher Scientific). As a control vector, a CSII-CMV-Venus vector plasmid was used for self-inactivating vector plasmid (SIN vector). The target sequences for shRNA were designed using siDirect version 2.0 web tool (http://sidirect2.rnai.jp/; Supplementary Table S1). A shRNA targeting luciferase was used as a control. Such shRNA sequences were inserted into a pENTR4-H1 vector, followed by transfer into a CS-RfA-CG vector plasmid using Gateway cloning technology. These

target vectors were co-transfected with pCAG-HIVgp and pCMV-VSV-G-RSV-Rev plasmids into HEK293T cells (ATCC) using polyethylenimine (PEI; Sigma–Aldrich, St. Louis, MO, USA) at a ratio of 1:5 (DNA:PEI, weight by weight). After 48 h of incubation, the supernatant containing virus was harvested, mixed with a Lenti-X Concentrator (Clontech Laboratories, Mountain View, CA, USA) and centrifuged at 1,500×g for 45 min at 4°C. The pellet was suspended in 1/100 of RPMI-1640 and stored at -80°C until use. CSII-CMV-RfA-IRES2-Venus, CSII-CMV-Venus, pENTR4-H1, CS-RfA-CG, pCAG-HIVgp, and pCMV-VSV-G-RSV-Rev plasmids were kindly provided by Dr. Hiroyuki Miyoshi and RIKEN BioResource Center. HUT102 or TL-Om1 cells were infected with viral product using 4 μg/mL of polybrene (Nacalai Tesque, Kyoto, Japan). Fluorescence-positive cells were sorted using BD FACS Aria II (BD Biosciences, San Jose, CA, USA) and collected.

***Quantitative RT-PCR analysis***

Total RNA was extracted from cells with TRIzol reagent (Thermo Fisher Scientific), followed by reverse-transcription with Prime Script RT Master Mix (Takara Bio, Kusatsu, Japan). TaqMan qPCR (Roche, Basel, Switzerland) and SYBR Green qPCR (Toyobo), performed a minimum of three times for each target gene. The expression levels of target genes were calculated using the delta-delta Ct method and normalized by the housekeeping gene, *GAPDH*. Oligonucleotide primers used for TaqMan PCR and SYBR Green qPCR assays are shown in Supplementary Table S1.

***Western blot analysis***

Cell lysates were extracted from ATL cells. A total of 50 μg of each protein sample was electrophoresed by 8% SDS–polyacrylamide gel electrophoresis and transferred to nitrocellulose

membranes. The membranes were incubated with the following antibodies as primary antibodies: anti-HGF (ab178395, Abcam, Cambridge, UK), anti–c-Met (#8198, Cell Signaling Technology, Danvers, MA, USA), anti–phospho–c-Met (#3088, Cell Signaling Technology), anti-Akt (#4691, Cell Signaling Technology), anti–phospho-Akt (#4060, Cell Signaling Technology), anti–Erk1/2 (#4695, Cell Signaling Technology), anti–phospho-Erk1/2 (#4370, Cell Signaling Technology), anti-Stat3 (#12640, Cell Signaling Technology), anti–phospho-Stat3 (#9145, Cell Signaling Technology), and anti–β-actin (#3700, Cell Signaling Technology). HRP-linked anti-rabbit IgG (#7074, Cell Signaling Technology) and HRP-linked anti-mouse IgG (#7076, Cell Signaling Technology) were used as secondary antibodies. Regarding c-Met internalization analysis, HUT102 cells were cultured with 20 μM MG132 (Cayman Chemical, Ann Arbor, MI, USA) and/or 100 nM concanamycin A (BioViotica Naturstoffe GmbH, Liestal, Switzerland) for 0, 0.5, 1, and 3 h. MT-1 and ATN-1 cells were cultured with 100 ng/mL HGF for 0, 0.25, 0.5, 1, 3, and 24 h. At each time point, protein was extracted from cells. The expression levels of c-Met and c-Met phosphorylation were analyzed by western blotting. Amersham ECL Select Western blotting detection reagent (12644055, GE Healthcare) was used for signal detection, and the density of bands was quantified by Image J software version 1.52a (https://imagej.nih.gov/ij/).

***Immunohistochemistry***

Specimens were fixed with 10% buffered formalin and embedded in paraffin. Immunohistochemical analysis was performed with anti-human CD4 (4B12, Leica Biosystems, Buffalo Grove, IL, USA), anti-human CD25 (4C9, Leica Biosystems), and anti-human HGF (ab178395, Abcam) antibodies. Images were obtained with an Olympus BX53 biological microscope and Olympus cellSens imaging software version 1.7.1 (Olympus Corporation, Tokyo, Japan). Tumor area was calculated by tracing hCD25-positive cells using Image J software. Areas

from multiple regions (at least three per specimen) were averaged.

***Cytokine and growth factor array analysis***

ATL cells were cultured overnight in fetal bovine serum (FBS)-free media. The expression profiles of 80 cytokines, chemokines, and growth factors in each ATL cell were analyzed with Human Cytokine Array C5 (RayBiotech, Peachtree Corners, GA, USA) in duplicate according to the manufacturer's instructions.

***Enzyme-Linked Immunosorbent Assay***

Concentrations of HGF and CCL2 in cell culture supernatants and/or sera from patients were measured by Quantikine ELISA Human HGF immunoassays (DHG00, R&D Systems, Minneapolis, MN, USA) and Human CCL2/MCP-1 Immunoassays (DCP00, R&D Systems), respectively, according to the manufacturer's instructions. The cell culture supernatants were collected after culturing the cells in serum deprived medium for 24 h.

***Cell proliferation and invasion assays***

Cells were seeded at a density of $2\times10^5$ cells per well. For the cell proliferation assay, 100 ng/mL recombinant human HGF (Pepro Tech, Rocky Hill, NJ, USA) was added every 24 h [22, 32, 37]. For cell proliferation assays, cells were treated with either BET inhibitor (JQ1, Selleck Chemicals, Houston, TX, USA), selective c-MET inhibitor (PHA-665752, Selleck Chemicals), or dimethyl sulfoxide (DMSO, Sigma–Aldrich) and counted in triplicate. Viable cells were assessed every 24 h using trypan blue staining. Cell invasion assays were performed using Corning BioCoat Matrigel Invasion Chambers with an 8.0 μm pore size (Corning, Corning, NY, USA). The lower chambers were filled with medium containing 10% FBS. Cells ($1\times10^6$) were

suspended in FBS-free medium and seeded into each Matrigel insert. HGF (100 ng/mL) or phosphate buffered saline was added to the lower chambers, and cells were incubated for 24 h. The number of infiltrating cells in the lower chambers was counted by trypan blue staining in triplicate.

***Apoptosis assay***

Cells were treated with JQ1 (0.25 μM) plus either pan-caspase inhibitor (10 μM, Z-VAD-FMK, MBL, Nagoya, Japan), caspase-3 inhibitor (10 μM, Z-DEVD-FMK, MBL), caspase-9 inhibitor (10 μM, Z-LEHD-FML, MBL), or DMSO in triplicate for 24 h followed by counting using trypan blue staining. Apoptotic cells were also evaluated by Annexin V and propidium iodide staining (APC Annexin V Apoptosis Detection Kit with PI, BioLegend, San Diego, CA, USA) followed by flow cytometry analysis (BD FACSCalibur, BD Biosciences). Cells in early stages of apoptosis, late stages, and both together were determined as Annexin V-positive/propidium iodide-negative cells, Annexin V-positive/propidium iodide-positive cells, and all Annexin V-positive cells, respectively.

***Chromatin immunoprecipitation assay***

ChIP assays were performed according to previously published methods [38]. Briefly, cells ($1\times10^6$) were treated with 1% formaldehyde for 8 min to crosslink histones to DNA. Chromatin was sonicated using Covaris S220 (Covaris, Moburn, MA, USA). Lysates were incubated overnight with 2 μL of anti-BRD4 antibodies (A301-985A50; Bethyl, Montgomery, TX, USA) or anti-H3K27Ac (39133; Active Motif, Carlsbad, CA, USA) coupled with 50 μL of sheep anti-mouse IgG M280 Dyna beads (11201D, Thermo Fisher Scientific). After centrifugation, the beads were washed, and protein–DNA complexes were eluted and treated with RNase followed by

proteinase K treatment. DNA was extracted by a conventional phenol/chloroform method. Ten percent of each lysate was used as an input control. Primer sets for ChIP–PCR are shown in Supplementary Table S1. The putative enhancer region was identified by the enrichment of H3K27Ac, H3K4me1 and BRD4 in blood cells by reference to the public database (ChIP–Atlas database, https://chip-atlas.org/)..

***Animal experiments***

TL-Om1-HGF-Venus, TL-Om1-Venus, and HUT102-Venus cells ($5\times10^6$) were suspended in 0.2 mL RPMI-1640. TL-Om1-HGF-Venus or TL-Om1-Venus cells were intraperitoneally (i.p.) injected into 6-week-old male NOG mice (n = 8 for each group; Central Institute for Experimental Animals, Kawasaki, Japan). Tumor formation was detected after 50 days of transplantation. HUT102-Venus cells were inoculated i.p. into NOG mice (n = 14). Of these, seven mice were treated with JQ1 and another seven mice treated with DMSO as a control. Seven days after inoculation, mice were treated with JQ1 (50 mg/kg i.p.) or DMSO five times weekly for three weeks. Seven days after inoculation, mice were treated with JQ1 (50 mg/kg i.p.) or DMSO five times weekly for three weeks. Mice were randomly assigned to the two groups. All experiments were performed under protocols approved by the Institutional Animal Care and Use Committee of Nagoya City University Graduate School of Medical Sciences (No. H30M-13). The sample size was determined to be the minimum number of animals that allowed the achievement of statistical rigor.

***Statistical analysis***

All statistical analysis was performed using GraphPad Prism 6 (GraphPad Software Inc., San Diego, CA, USA). The statistical significance of differences between two groups was analyzed

by paired Student's *t*-test, and differences between three groups were analyzed by one-way analysis of variance or a Kruskal–Wallis test. Survival was compared by the Kaplan–Meier method using a log-rank and Wilcoxon test. All reported *P*-values were two-sided, and $P < 0.05$ was considered statistically significant.

**Acknowledgments**

This study was performed as research program with a Grant-in-Aid for Scientific Research from the Japan Society for the Promotion of Science (25290048, Y. Kondo; 19K16752, H. Totani) and the National Cancer Center Research and Development Fund (29-A-3, S. Iida).

**Conflict of interest**

The authors disclose no potential conflicts of interest.

**Author contributions**

Conception and design: H.T., Y.K.; development of methodology: H.T., K.S., M.S., K.K., A.M., A.I., Y.K.; acquisition of data: H.T., K.S., M.S., K.K., S.M., A.M., A.I., M.R., S.K., H.K., H.I., T.I., S.I., Y.K.; analysis and interpretation of data: H.T., K.S., M.S., A.M., A.I., T.I, H.I., S.I., Y.K.; writing of the manuscript: H.T., Y.K.; administrative, technical, or material support: T.I., H.I., S.I., Y.K.

Supplementary information is available at *Oncogene*'s website.

## References


1 Uchiyama T, Yodoi J, Sagawa K, Takatsuki K, Uchino H. Adult T-cell leukemia: clinical and hematologic features of 16 cases. *Blood* 1977; 50: 481-492.

2 Poiesz BJ, Ruscetti FW, Gazdar AF, Bunn PA, Minna JD, Gallo RC. Detection and isolation of type C retrovirus particles from fresh and cultured lymphocytes of a patient with cutaneous T-cell lymphoma. *Proc Natl Acad Sci U S A* 1980; 77: 7415-7419.

3 Hinuma Y, Nagata K, Hanaoka M, Nakai M, Matsumoto T, Kinoshita KI *et al.* Adult T-cell leukemia: antigen in an ATL cell line and detection of antibodies to the antigen in human sera. *Proc Natl Acad Sci U S A* 1981; 78: 6476-6480.

4 Shimoyama M. Diagnostic criteria and classification of clinical subtypes of adult T-cell leukaemia-lymphoma. A report from the Lymphoma Study Group (1984-87). *Br J Haematol* 1991; 79: 428-437.

5 Katsuya H, Ishitsuka K, Utsunomiya A, Hanada S, Eto T, Moriuchi Y *et al.* Treatment and survival among 1594 patients with ATL. *Blood* 2015; 126: 2570-2577.

6 Yamada Y, Kamihira S, Murata K, Yamamura M, Maeda T, Tsukasaki K *et al.* Frequent hepatic involvement in adult T cell leukemia: comparison with non-Hodgkin's lymphoma. *Leuk Lymphoma* 1997; 26: 327-335.

7 Yoshie O, Fujisawa R, Nakayama T, Harasawa H, Tago H, Izawa D *et al.* Frequent expression of CCR4 in adult T-cell leukemia and human T-cell leukemia virus type 1-transformed T cells. *Blood* 2002; 99: 1505-1511.

8 Hieshima K, Nagakubo D, Nakayama T, Shirakawa AK, Jin Z, Yoshie O. Tax-inducible production of CC chemokine ligand 22 by human T cell leukemia virus type 1 (HTLV-1)-infected T cells promotes preferential transmission of HTLV-1 to CCR4-expressing CD4+ T cells. *J Immunol* 2008; 180: 931-939.

9 Ishida T, Joh T, Uike N, Yamamoto K, Utsunomiya A, Yoshida S *et al.* Defucosylated anti-CCR4 monoclonal antibody (KW-0761) for relapsed adult T-cell leukemia-

lymphoma: a multicenter phase II study. *J Clin Oncol* 2012; 30: 837-842.

10 Ishida T, Jo T, Takemoto S, Suzushima H, Uozumi K, Yamamoto K *et al.* Dose-intensified chemotherapy alone or in combination with mogamulizumab in newly diagnosed aggressive adult T-cell leukaemia-lymphoma: a randomized phase II study. *Br J Haematol* 2015; 169: 672-682.

11 Ishida T, Utsunomiya A, Jo T, Yamamoto K, Kato K, Yoshida S *et al.* Mogamulizumab for relapsed adult T-cell leukemia-lymphoma: Updated follow-up analysis of phase I and II studies. *Cancer Sci* 2017; 108: 2022-2029.

12 Umino A, Nakagawa M, Utsunomiya A, Tsukasaki K, Taira N, Katayama N *et al.* Clonal evolution of adult T-cell leukemia/lymphoma takes place in the lymph nodes. *Blood* 2011; 117: 5473-5478.

13 Kataoka K, Nagata Y, Kitanaka A, Shiraishi Y, Shimamura T, Yasunaga J *et al.* Integrated molecular analysis of adult T cell leukemia/lymphoma. *Nat Genet* 2015; 47: 1304-1315.

14 Yamagishi M, Nakano K, Miyake A, Yamochi T, Kagami Y, Tsutsumi A *et al.* Polycomb-mediated loss of miR-31 activates NIK-dependent NF-kappaB pathway in adult T cell leukemia and other cancers. *Cancer Cell* 2012; 21: 121-135.

15 Fujikawa D, Nakagawa S, Hori M, Kurokawa N, Soejima A, Nakano K *et al.* Polycomb-dependent epigenetic landscape in adult T-cell leukemia. *Blood* 2016; 127: 1790-1802.

16 Yamagishi M, Hori M, Fujikawa D, Ohsugi T, Honma D, Adachi N *et al.* Targeting Excessive EZH1 and EZH2 Activities for Abnormal Histone Methylation and Transcription Network in Malignant Lymphomas. *Cell Rep* 2019; 29: 2321-2337 e2327.

17 Ding X, Ji J, Jiang J, Cai Q, Wang C, Shi M *et al.* HGF-mediated crosstalk between cancer-associated fibroblasts and MET-unamplified gastric cancer cells activates coordinated tumorigenesis and metastasis. *Cell Death Dis* 2018; 9: 867.

18 Hartmann S, Bhola NE, Grandis JR. HGF/Met Signaling in Head and Neck Cancer: Impact on the Tumor Microenvironment. *Clin Cancer Res* 2016; 22: 4005-4013.

19 Kwon Y, Smith BD, Zhou Y, Kaufman MD, Godwin AK. Effective inhibition of c-MET-mediated signaling, growth and migration of ovarian cancer cells is influenced by the ovarian tissue microenvironment. *Oncogene* 2015; 34: 144-153.

20 Choi YL, Tsukasaki K, O'Neill MC, Yamada Y, Onimaru Y, Matsumoto K *et al.* A genomic analysis of adult T-cell leukemia. *Oncogene* 2007; 26: 1245-1255.

21 Imaizumi Y, Murota H, Kanda S, Hishikawa Y, Koji T, Taguchi T *et al.* Expression of the c-Met proto-oncogene and its possible involvement in liver invasion in adult T-cell leukemia. *Clin Cancer Res* 2003; 9: 181-187.

22 Onimaru Y, Tsukasaki K, Murata K, Imaizumi Y, Choi YL, Hasegawa H *et al.* Autocrine and/or paracrine growth of aggressive ATLL cells caused by HGF and c-Met. *Int J Oncol* 2008; 33: 697-703.

23 Oki S, Ohta T, Shioi G, Hatanaka H, Ogasawara O, Okuda Y *et al.* ChIP-Atlas: a data-mining suite powered by full integration of public ChIP-seq data. *EMBO Rep* 2018; 19.

24 Oshiro A, Tagawa H, Ohshima K, Karube K, Uike N, Tashiro Y *et al.* Identification of subtype-specific genomic alterations in aggressive adult T-cell leukemia/lymphoma. *Blood* 2006; 107: 4500-4507.

25 Piekarz RL, Frye R, Turner M, Wright JJ, Allen SL, Kirschbaum MH *et al.* Phase II multi-institutional trial of the histone deacetylase inhibitor romidepsin as monotherapy for patients with cutaneous T-cell lymphoma. *J Clin Oncol* 2009; 27: 5410-5417.

26 Piekarz RL, Frye R, Prince HM, Kirschbaum MH, Zain J, Allen SL *et al.* Phase 2 trial of romidepsin in patients with peripheral T-cell lymphoma. *Blood* 2011; 117: 5827-5834.

27 Olsen EA, Kim YH, Kuzel TM, Pacheco TR, Foss FM, Parker S *et al.* Phase IIb

multicenter trial of vorinostat in patients with persistent, progressive, or treatment refractory cutaneous T-cell lymphoma. *J Clin Oncol* 2007; 25: 3109-3115.

28 Nakagawa M, Shaffer AL, 3rd, Ceribelli M, Zhang M, Wright G, Huang DW *et al.* Targeting the HTLV-I-Regulated BATF3/IRF4 Transcriptional Network in Adult T Cell Leukemia/Lymphoma. *Cancer Cell* 2018; 34: 286-297 e210.

29 Rutella S, Bonanno G, Procoli A, Mariotti A, de Ritis DG, Curti A *et al.* Hepatocyte growth factor favors monocyte differentiation into regulatory interleukin (IL)-10++IL-12low/neg accessory cells with dendritic-cell features. *Blood* 2006; 108: 218-227.

30 Bonanno G, Mariotti A, Procoli A, Folgiero V, Natale D, De Rosa L *et al.* Indoleamine 2,3-dioxygenase 1 (IDO1) activity correlates with immune system abnormalities in multiple myeloma. *J Transl Med* 2012; 10: 247.

31 Masaki A, Ishida T, Maeda Y, Suzuki S, Ito A, Takino H *et al.* Prognostic Significance of Tryptophan Catabolism in Adult T-cell Leukemia/Lymphoma. *Clin Cancer Res* 2015; 21: 2830-2839.

32 Skibinski G, Skibinska A, James K. Hepatocyte growth factor (HGF) protects c-met-expressing Burkitt's lymphoma cell lines from apoptotic death induced by DNA damaging agents. *Eur J Cancer* 2001; 37: 1562-1569.

33 Miyoshi I, Kubonishi I, Sumida M, Hiraki S, Tsubota T, Kimura I *et al.* A novel T-cell line derived from adult T-cell leukemia. *Gan* 1980; 71: 155-156.

34 Sugamura K, Fujii M, Kannagi M, Sakitani M, Takeuchi M, Hinuma Y. Cell surface phenotypes and expression of viral antigens of various human cell lines carrying human T-cell leukemia virus. *Int J Cancer* 1984; 34: 221-228.

35 Naoe T, Akao Y, Yamada K, Utsumi KR, Koike K, Shamoto M *et al.* Cytogenetic characterization of a T-cell line, ATN-1, derived from adult T-cell leukemia cells. *Cancer Genet Cytogenet* 1988; 34: 77-88.

36 Suzuki S, Masaki A, Ishida T, Ito A, Mori F, Sato F *et al.* Tax is a potential

molecular target for immunotherapy of adult T-cell leukemia/lymphoma. *Cancer Sci* 2012; 103: 1764-1773.

37 Xu C, Plattel W, van den Berg A, Ruther N, Huang X, Wang M *et al.* Expression of the c-Met oncogene by tumor cells predicts a favorable outcome in classical Hodgkin's lymphoma. *Haematologica* 2012; 97: 572-578.

38 Murashima A, Shinjo K, Katsushima K, Onuki T, Kondoh Y, Osada H *et al.* Identification of a chemical modulator of EZH2-mediated silencing by cell-based high-throughput screening assay. *J Biochem* 2019; 166: 41-50.

**Figure legends**

**Figure 1. Expression of HGF in ATL cell lines and clinical samples**

A, Cytokine and growth factor arrays containing 80 cytokines and growth factors were performed in HUT102 (lymph node adult T-cell leukemia/lymphoma [LN-ATL]), MT-1, TL-Om1, and ATN-1 (peripheral blood adult T-cell leukemia/lymphoma [PB-ATL]) cell lines. The four dots at the top left, two dots on the bottom right, and two dots at the top middle represent positive and negative controls for experiments, respectively. B, Amounts of HGF and CCL2 in cell culture supernatants quantified by ELISA. Error bars indicate standard deviations (SD). $^{**}P < 0.01$. C, The mRNA expression levels of ligands (*HGF* and *CCL2*) and their corresponding membrane receptors, *c-Met* and *CCR2*, in ATL cell lines (HUT102, MT-1, TL-Om1, and ATN-1), a human T-cell leukemia virus type I (HTLV-1)–immortalized cell line (TL-Su), and normal CD4+ cells. The *y*-axis indicates the relative mRNA levels of each gene normalized to that of *GAPDH*. Error bars indicate SD. D, Hepatocyte growth factor (HGF) protein expression in two representative patients with clinical ATL (Pt. 9 and Pt. 13 in Table 1). Hematoxylin eosin (HE) staining (upper panels), immunohistochemical staining of CD4 (middle panels), and HGF (lower panels) were performed in the peripheral blood, and lymph node or pharynx. Scale bars indicate 50 μm.

**Figure 2. HGF promotes ATL cell proliferation and invasion**

A, Cell proliferation analysis after HGF (100 ng/mL) or phosphate buffered saline (PBS) treatment, three times every 24 h, in MT-1 and TL-Om1 cell lines (top). Viable cell numbers were counted by trypan blue staining (bottom). Squares indicate cells treated with HGF, and circles indicate control cells. The *y*-axis indicates cell number relative to control at 0 h. Error bars indicate SD. $^{**}P < 0.01$. B, Cell proliferation analysis in ATL cells, with and without HGF overexpression. HGF protein expression in stable cell lines overexpressing HGF (OE) and vector control (Ctrl;

top). Viable cell numbers were counted by trypan blue staining (bottom). Squares indicate HGF overexpressing cells, and circles indicate control cells. The *y*-axis indicates the cell number relative to control at 0 h. Error bars indicate SD. **P* < 0.05, ***P* < 0.01. C, Depletion of HGF in HUT102 by two independent short hairpin (sh)RNA sequences (shHGF #1 and shHGF #2, top left). The protein expression levels of HGF and β-actin (loading control) were quantified and calculated as HGF/β-actin ratios (top right). The bar graph shows relative cell numbers in sh-control (shCtrl, black), shHGF #1 (right gray), and shHGF #2 (dark gray) at 24 and 48 h (bottom). Error bars indicate SD. **P* < 0.05, ***P* < 0.01. D, E, Cell invasion assay with HGF treatment (D) or HGF overexpression (E). The number of infiltrating cells was counted after HGF treatment (100 ng/mL) or overexpression (gray), or PBS treatment (black). The *y*-axis indicates cell number after HGF treatment relative to that of control. Error bars indicate SD. ***P* < 0.01. Scale bars indicate 100 μm. F, 6-week-NOG mice were intraperitoneally injected with $5\times10^6$ HGF-overexpressing (TL-Om1-HGF-Venus) or control (TL-Om1-Venus; n = 8, each group) cells. Tumor formation was confirmed after 50 days of transplantation. The appearance of mice (top), laparotomy (middle), and spleen (bottom) in control (Ctrl) and HGF overexpression (OE) groups. The arrowhead indicates the tumor. G, Weights of tumors, livers, and ascites, and weights and area of spleens in mice (Ctrl and OE, n=8 and 8, respectively) shown in F. Error bars indicate SD. ***P* < 0.01. n = 8. H, HE staining and immunohistochemistry with anti-human CD4 in livers and spleens of mice in F. Scale bars indicate 100 μm.

**Figure 3. Effects of HGF/c-Met signaling and its downstream pathway on ATL cell growth**

A, HGF/c-Met signaling pathway in each ATL cell line. After 15 min HGF treatment (100 ng/mL), cellular protein was examined by western blotting. The quantification of bands is shown as values under the bands (left). Experiments were performed in triplicate and the data calculated is shown

in bar graphs (right). The *y*-axis indicates a mean relative ratio of phosphorylated to total amount of each protein expressed, with (gray) and without (black) HGF treatment. Error bars indicate SD. $^{**}P < 0.01$. *N.S.*, not significant. B, HGF/c-Met signaling pathway in HGF-overexpressing TL-Om1 cells. The quantification of bands is shown as values under the bands (left). Experiments were performed in triplicate and data is shown in bar graphs (right). The *y*-axis indicates the mean relative ratio of phosphorylated to total amount of each protein expressed in control (black) and HGF-overexpressing cells (gray). Error bars indicate SD. $^{*}P < 0.05$, $^{**}P < 0.01$. *N.S.*, not significant. C, Effects of c-Met inhibitor (PHA-665752) on the downstream signal in HUT102 cells after 6 h of treatment. Values under the bands indicate the relative ratio of phosphorylated to total amount of each protein expressed (left). The *y*-axis indicates the mean relative ratio of phosphorylated to total amount of each protein expressed (right). Error bars indicate SD. $^{**}P < 0.01$. D, The numbers of viable HUT102 cells treated with PBS (Ctrl, black), PHA-665752 (right gray), and PHA-665752 plus HGF (100 ng/mL) for 72 h. The *y*-axis indicates cell number relative to control. HGF was added every 24 h. Error bars indicate SD. $^{*}P < 0.05$, $^{**}P < 0.01$. E, Phosphorylated Akt/Akt after treatment of PHA-665752, with or without HGF (100 ng/mL). The values under the bands (left) and the bar graphs indicate the mean relative ratio of phosphorylated to total amount of each protein expressed after treatment with PHA-665752, with or without HGF (right). Error bars indicate SD. $^{**}P < 0.01$.

**Figure 4. Regulation of HGF expression by epigenetic mechanisms**

A, Schema of *HGF* promoter (P) and enhancer (E) regions. B, Chromatin immunoprecipitation (ChIP–PCR) analyses of BRD4 and H3K27Ac in the *HGF* promoter (P) and enhancer (E) regions. HUT102 and TL-Om1 cell lines were treated with JQ1 (gray, 0.25 μM) or control (dimethylsulfoxide, black). Error bars indicate SD. $^{*}P < 0.05$, $^{**}P < 0.01$. *N.S.*, not significant.

C, The expression level of *HGF* mRNA. HUT102 cells were treated with JQ1 at 0, 0.25, or 0.5 μM for 48 h. The *y*-axis indicates the relative ratio of *HGF* to *GAPDH* expression. Error bars indicate SD. ***P* < 0.01. D, Effects of JQ1 on the HGF/c-Met signaling pathway after 72 h of treatment. The values under the HGF bands indicate the relative ratio of HGF to β-actin expression or relative expression ratio of the phosphorylated to total amount of each protein (left). Experiments were conducted in triplicates and data are shown in bar graphs (right). Error bars indicate SD. **P* < 0.05, ***P* < 0.01. E, The viable cell number after treatment with JQ1 was evaluated by trypan blue staining (top). The *y*-axis indicates cell number relative to control. Values under the bands indicate the relative ratio of phosphorylated Akt to total amount of Akt expression (bottom). Experiments were conducted in triplicate and the data calculated is shown in bar graphs (right). Short and long indicate short and long exposure times for signal detection by ECL, respectively. Error bars indicate SD. ***P* < 0.01. F, The number of viable cells after treatment with 0.25 μM JQ1 or JQ1 plus caspase inhibitors for 24 h. Z-VAD-FMK, Z-DEVD-FMK, and Z-LEHD-FMK were used as pan-caspase inhibitor, caspase-3 inhibitor, and caspase-9 inhibitor, respectively (all at 10 μM). The *y*-axis indicates cell number relative to control. Error bars indicate SD. * *P* < 0.05, ***P* < 0.01. G, Percentage of apoptotic cells after treatment with JQ1 or JQ1 plus caspase inhibitors. The *y*-axis indicates percentage of apoptotic cells. Error bars indicate SD. ***P* < 0.01. H, Treatment schema for JQ1. Six-week-old NOG mice were intraperitoneally injected with $5\times10^6$ HUT102 cells. After seven days of transplantation, PBS or JQ1 (5 mg/kg) was intraperitoneally injected five times a week for three weeks. The therapeutic effect was evaluated 30 days after transplantation (n = 6, each group). I, Mice appearances (top), laparotomy (middle), and spleen (bottom) in control (Ctrl) and JQ1 treatment groups. Arrowheads indicate a tumor. J, Effect of tumor reduction by JQ1. Error bars indicate SD. ***P* < 0.01. n = 6. K, HE staining (top), immunohistochemical staining of human (h) CD4 (middle), and hCD25 (bottom) in ATL tumors.

Scale bars indicate 50 μm. The right-hand panel shows the tumor area relative to the control group. Error bars indicate SD. **P* < 0.05. n = 6.

**Figure 5. Serum HGF expression in clinical samples**

A, Levels of HGF in sera from 51 patients with ATL (acute type: n = 38, lymphoma type: n = 13) and from 10 non-leukemic, healthy patients. The median and mean HGF levels are indicated by a solid horizontal line in the box and the "+", respectively. The box ends denote upper and lower quartiles. The whiskers represent minimum and maximum values. **P* < 0.05. B, Serum HGF levels of patients with ATL. Box-and-whisker plots represent patients with (n = 43) and without (n = 8) non-PB lesions. **P* < 0.05. C, Progression-free survival (PFS) and overall survival (OS) of 26 ATL patients with non-PB lesions who received mogamulizumab treatment. The reference date was defined as the starting date of mogamulizumab administration. Patients with ATL were divided into two groups according to the mean value of HGF (1.80 ng/mL), low (n = 15) and high (n = 11), respectively. Survival was calculated by the Kaplan–Meier method with log-rank and Wilcoxon tests.

**Table 1. HGF expression in 15 ATL patients with non-PB lesions**

| Case | Age | Sex | ATL type | non-PB lesion | | PB lesion | Serum HGF (ng/mL) |
|---|---|---|---|---|---|---|---|
| | | | | ATL tumor location | HGF expression | HGF expression | |
| 1 | 67 | female | lymphoma | small intestine | - | - | NA |
| 2 | 74 | female | acute | lymph node | + | + | NA |
| 3 | 65 | male | lymphoma | lymph node | ++ | NA | NA |
| 4 | 60 | female | acute | lymph node | + | - | NA |
| 5 | 60 | female | lymphoma | lymph node | - | NA | NA |
| 6 | 58 | male | acute | lymph node | + | NA | 0.82 |
| 7 | 59 | female | lymphoma | lymph node | + | NA | 0.71 |
| 8 | 71 | female | acute | lymph node | - | NA | 1.08 |
| 9 | 68 | female | acute | lymph node | + | + | 1.64 |
| 10 | 57 | female | lymphoma | pharynx | + | NA | 1.36 |
| 11 | 48 | male | lymphoma | lymph node | - | NA | 1.18 |
| 12 | 68 | male | acute | tongue | ++ | + | 6.03 |
| 13 | 68 | female | acute | pharynx | + | - | NA |
| 14 | 72 | male | acute | tonsil | ++ | NA | 2.24 |
| 15 | 76 | female | acute | bone marrow | ++ | + | NA |

-, no positive cells; +, less than 5% of positive cells; ++, more than 5% of positive cells; NA, not available.

# Figure 1

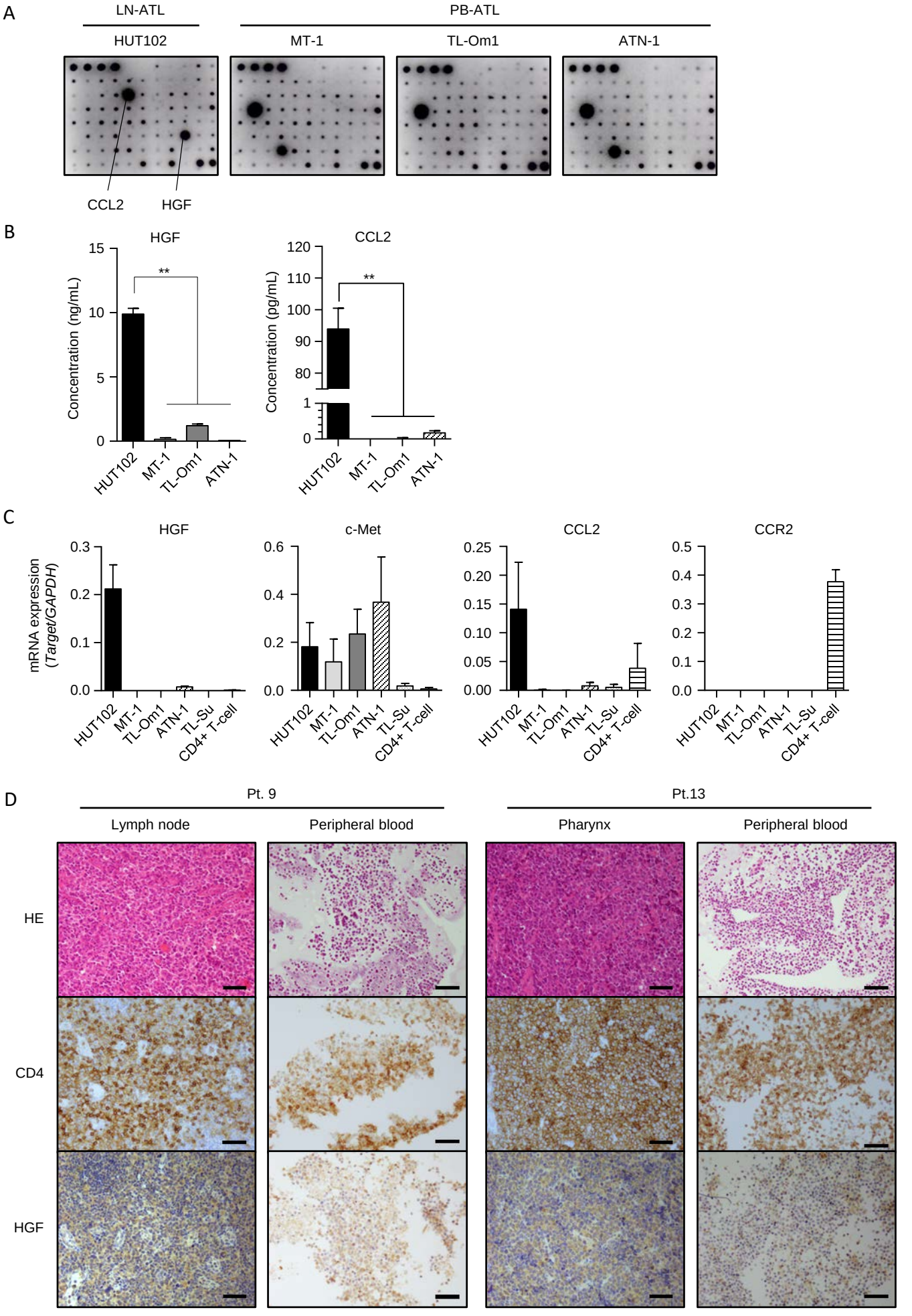
A
LN-ATL
PB-ATL
HUT102
MT-1
TL-Om1
ATN-1
CCL2
HGF
B
HGF
CCL2
Concentration (ng/mL)
Concentration (pg/mL)
**
**
HUT102
MT-1
TL-Om1
ATN-1
C
HGF
c-Met
CCL2
CCR2
mRNA expression (Target/GAPDH)
HUT102
MT-1
TL-Om1
ATN-1
TL-Su
CD4+ T-cell
D
Pt. 9
Pt.13
Lymph node
Peripheral blood
Pharynx
Peripheral blood
HE
CD4
HGF

# Figure 2

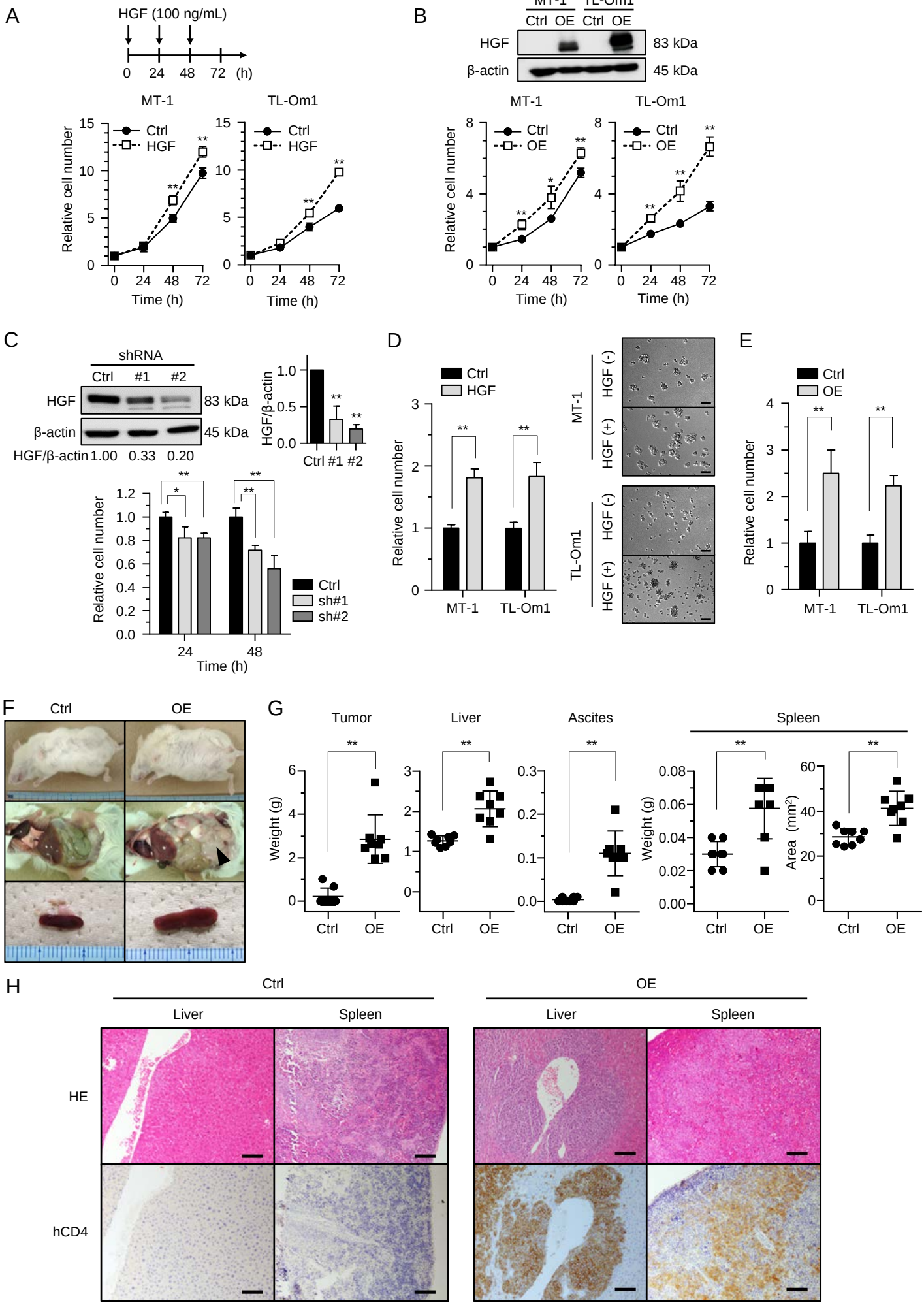
A
HGF (100 ng/mL)
0 24 48 72 (h)
MT-1
TL-Om1
Ctrl
HGF
Relative cell number
Time (h)
B
MT-1 TL-Om1
Ctrl OE Ctrl OE
HGF
β-actin
83 kDa
45 kDa
Ctrl
OE
C
shRNA
Ctrl #1 #2
HGF
β-actin
HGF/β-actin 1.00 0.33 0.20
HGF/β-actin
sh#1
sh#2
D
HGF (-)
HGF (+)
E
F
Ctrl
OE
G
Tumor
Liver
Ascites
Spleen
Weight (g)
Area (mm²)
H
Liver
Spleen
HE
hCD4

# Figure 3

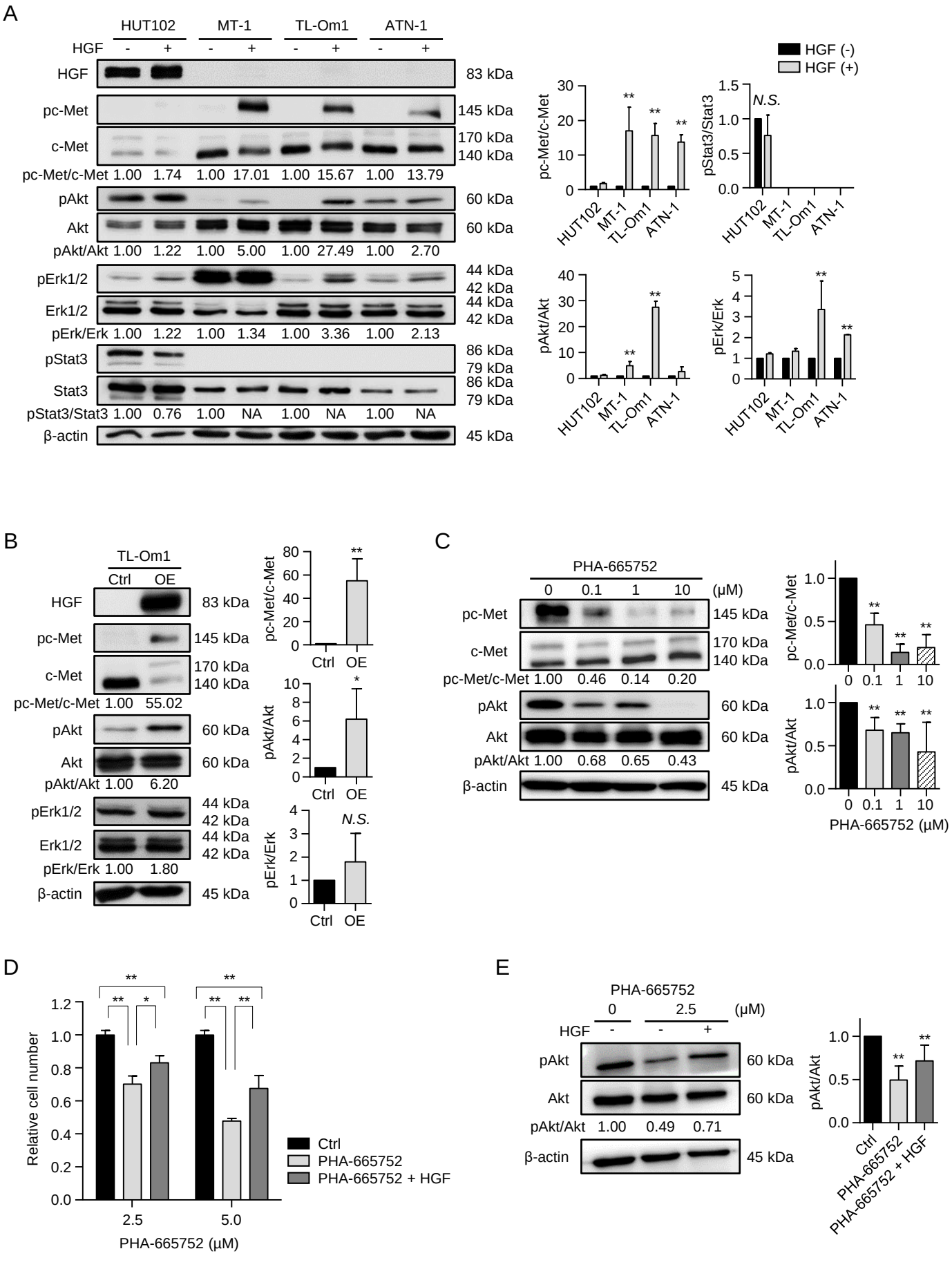
A
HUT102
MT-1
TL-Om1
ATN-1
HGF - + - + - + - +
HGF
pc-Met
c-Met
pc-Met/c-Met 1.00 1.74 1.00 17.01 1.00 15.67 1.00 13.79
pAkt
Akt
pAkt/Akt 1.00 1.22 1.00 5.00 1.00 27.49 1.00 2.70
pErk1/2
Erk1/2
pErk/Erk 1.00 1.22 1.00 1.34 1.00 3.36 1.00 2.13
pStat3
Stat3
pStat3/Stat3 1.00 0.76 1.00 NA 1.00 NA 1.00 NA
β-actin
83 kDa
145 kDa
170 kDa
140 kDa
60 kDa
60 kDa
44 kDa
42 kDa
44 kDa
42 kDa
86 kDa
79 kDa
86 kDa
79 kDa
45 kDa
HGF (-)
HGF (+)
pc-Met/c-Met
pStat3/Stat3
N.S.
pAkt/Akt
pErk/Erk
B
TL-Om1
Ctrl OE
HGF
pc-Met
c-Met
pc-Met/c-Met 1.00 55.02
pAkt
Akt
pAkt/Akt 1.00 6.20
pErk1/2
Erk1/2
pErk/Erk 1.00 1.80
β-actin
C
PHA-665752
0 0.1 1 10 (μM)
pc-Met
c-Met
pc-Met/c-Met 1.00 0.46 0.14 0.20
pAkt
Akt
pAkt/Akt 1.00 0.68 0.65 0.43
β-actin
PHA-665752 (μM)
D
Relative cell number
Ctrl
PHA-665752
PHA-665752 + HGF
2.5
5.0
PHA-665752 (μM)
E
PHA-665752
0 2.5 (μM)
HGF - - +
pAkt
Akt
pAkt/Akt 1.00 0.49 0.71
β-actin
Ctrl
PHA-665752
PHA-665752 + HGF

# Figure 4

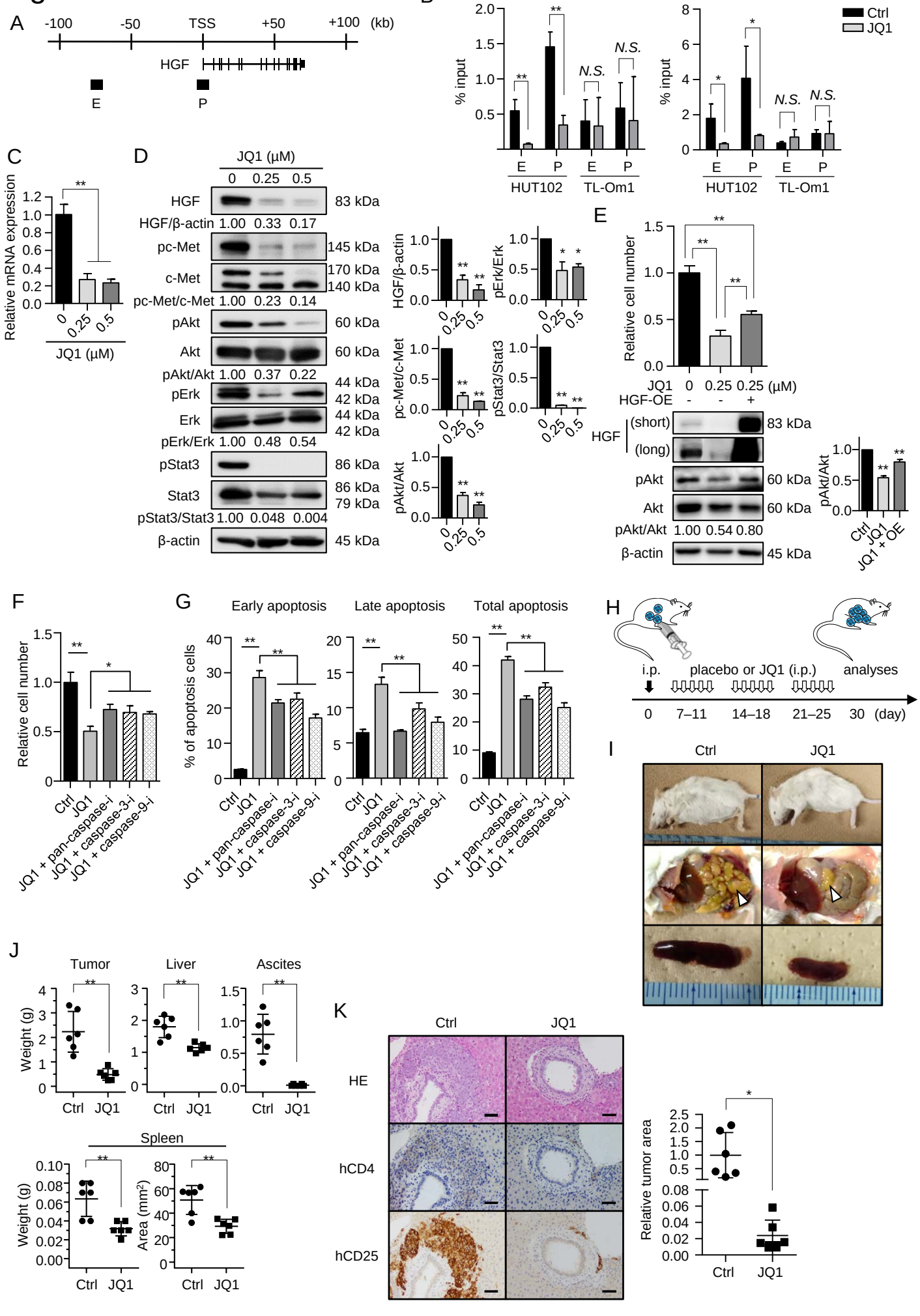
A
-100
-50
TSS
+50
+100
(kb)
HGF
E
P
B
BRD4
H3K27Ac
Ctrl
JQ1
% input
N.S.
HUT102
TL-Om1
C
Relative mRNA expression
JQ1 (μM)
D
JQ1 (μM)
HGF
HGF/β-actin 1.00 0.33 0.17
pc-Met
c-Met
pc-Met/c-Met 1.00 0.23 0.14
pAkt
Akt
pAkt/Akt 1.00 0.37 0.22
pErk
Erk
pErk/Erk 1.00 0.48 0.54
pStat3
Stat3
pStat3/Stat3 1.00 0.048 0.004
β-actin
83 kDa
145 kDa
170 kDa
140 kDa
60 kDa
44 kDa
42 kDa
86 kDa
79 kDa
45 kDa
HGF/β-actin
pErk/Erk
pc-Met/c-Met
pStat3/Stat3
pAkt/Akt
E
Relative cell number
JQ1 0 0.25 0.25 (μM)
HGF-OE - - +
HGF (short)
HGF (long)
pAkt
Akt
pAkt/Akt 1.00 0.54 0.80
β-actin
83 kDa
60 kDa
60 kDa
45 kDa
Ctrl
JQ1
JQ1 + OE
F
Relative cell number
Ctrl
JQ1
JQ1 + pan-caspase-i
JQ1 + caspase-3-i
JQ1 + caspase-9-i
G
Early apoptosis
Late apoptosis
Total apoptosis
% of apoptosis cells
H
i.p.
placebo or JQ1 (i.p.)
analyses
0
7–11
14–18
21–25
30 (day)
I
Ctrl
JQ1
J
Tumor
Liver
Ascites
Weight (g)
Spleen
Area (mm²)
K
Ctrl
JQ1
HE
hCD4
hCD25
Relative tumor area

# Figure 5

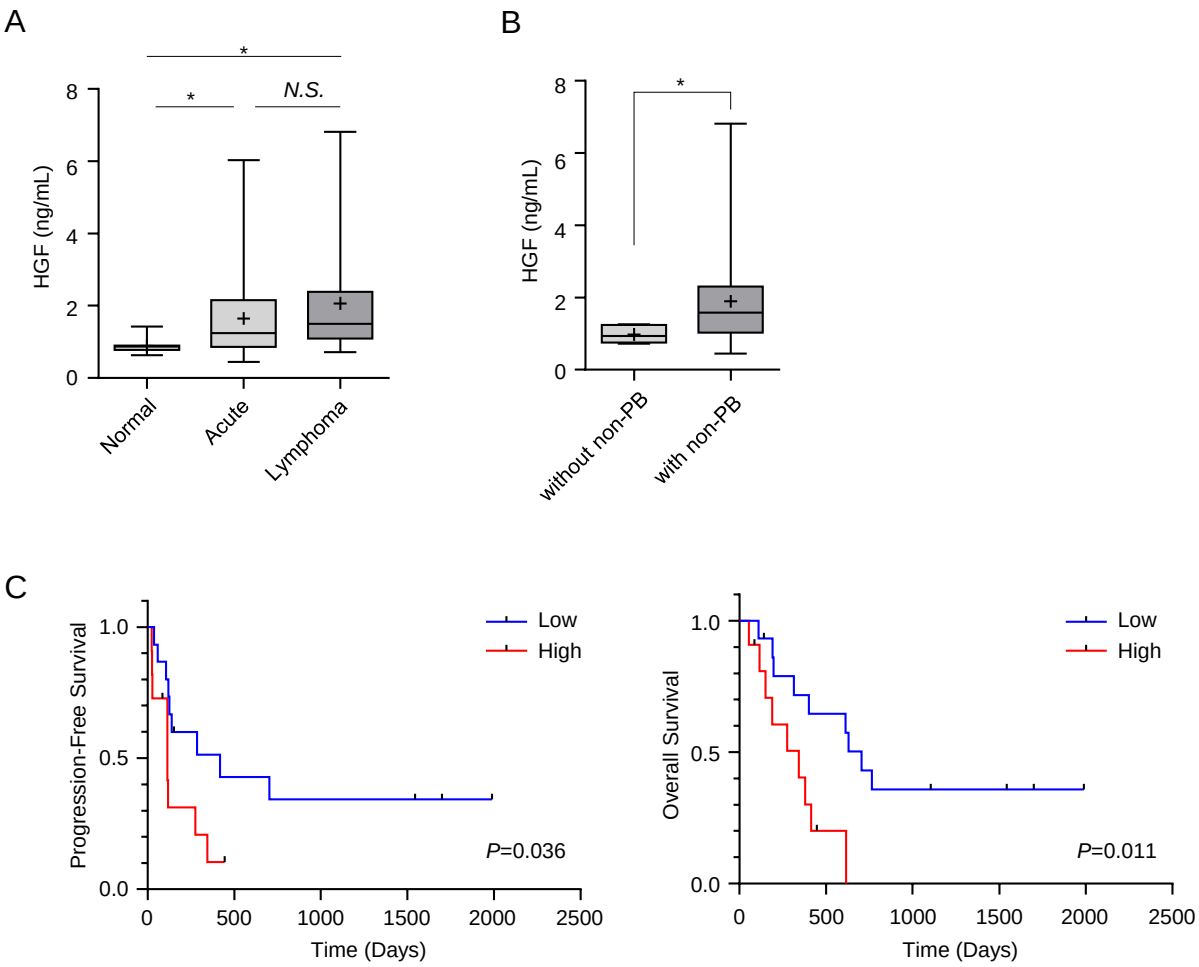
A
B
C
HGF (ng/mL)
Normal
Acute
Lymphoma
N.S.
without non-PB
with non-PB
Progression-Free Survival
Overall Survival
Time (Days)
Low
High
P=0.036
P=0.011

# Supplementary Figure S1

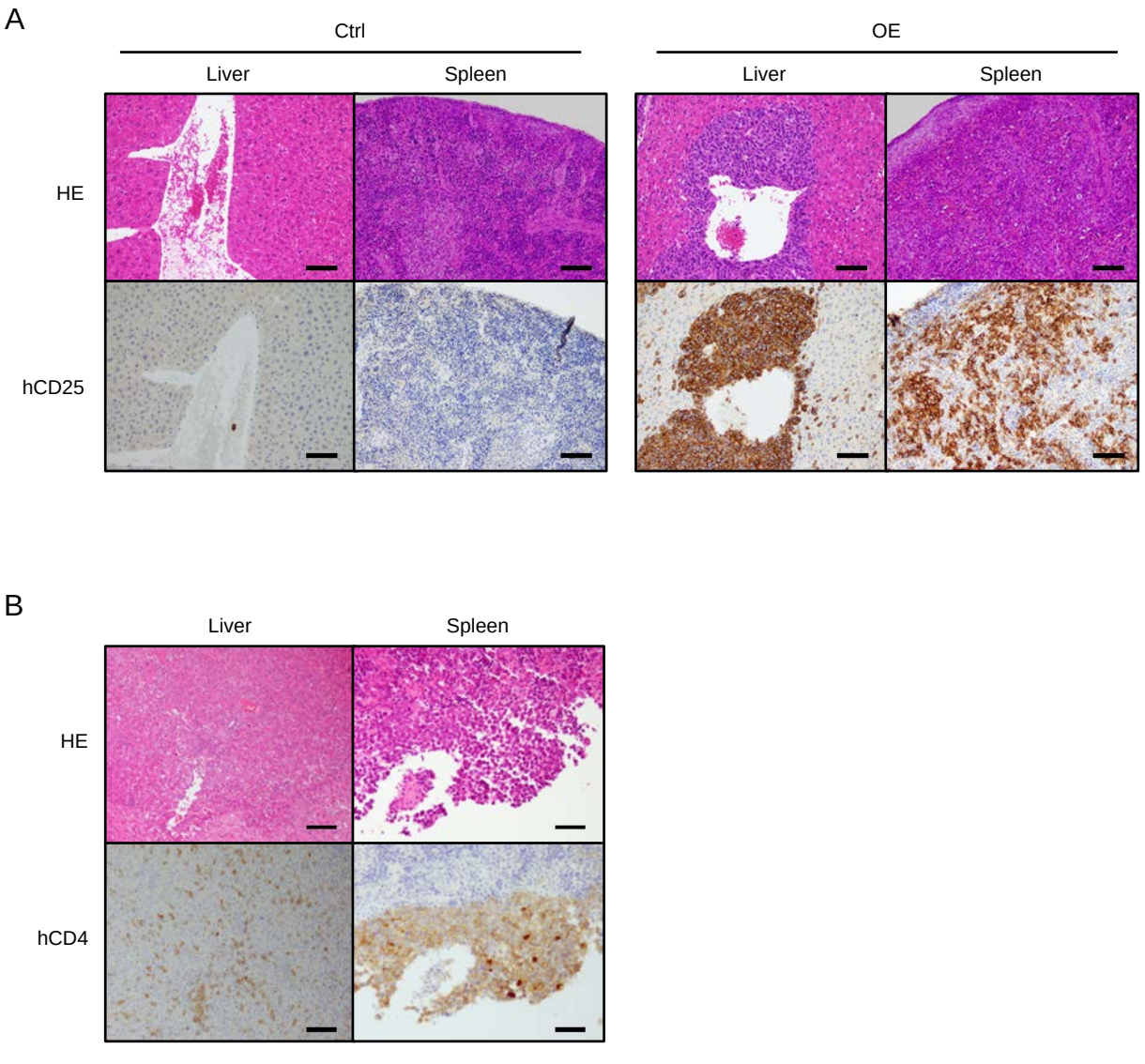

# Supplementary Figure S2

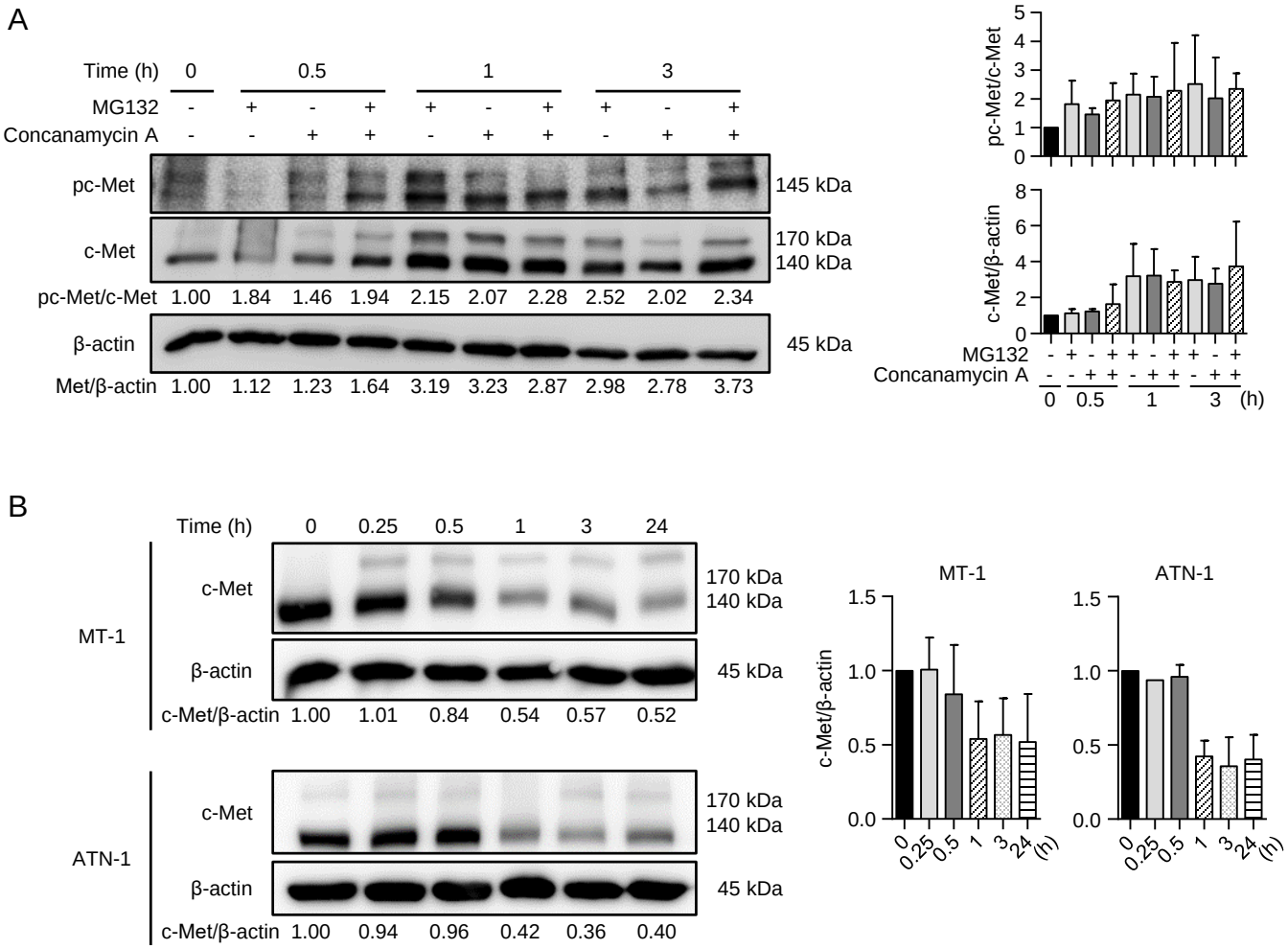

# Supplementary Figure S3

A

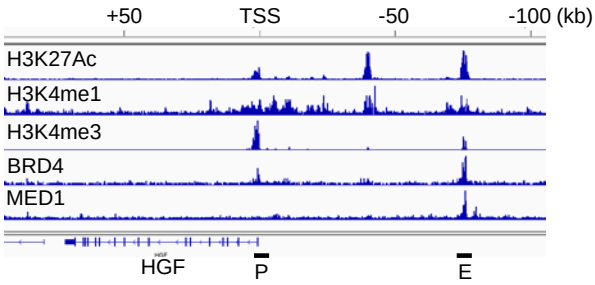


B

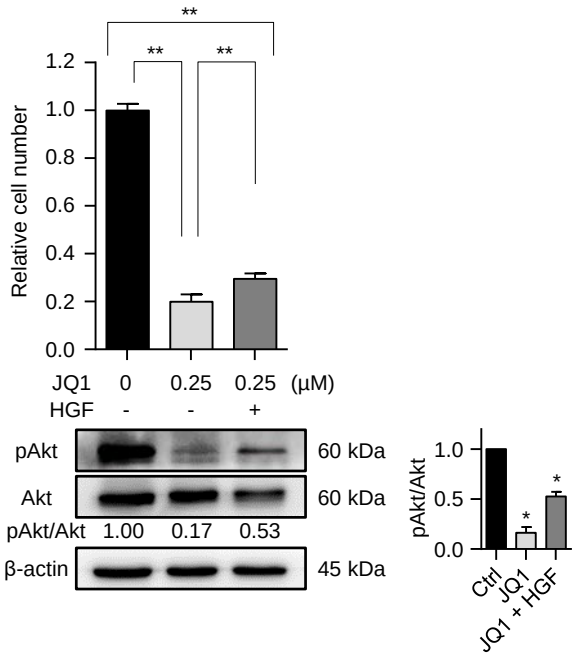

**Supplementary Figure legends**

**Supplementary Fig. S1. Organ invasion by HGF-overexpressing ATL cells**

A, Tumorigenesis and organ invasion by hepatocyte growth factor (HGF)-overexpressing TL-Om1 cells. Hematoxylin and eosin (HE) staining and immunohistochemical staining of anti-human (h) CD25 in the livers and spleens of mice in Fig. F. Scale bars indicate 100 μm. B, HE staining and immunohistochemistry with anti-hCD4 in liver and spleen. Scale bars indicate 100 μm.

**Supplementary Fig. S2. Internalization of c-Met protein after HGF stimulation**

A, After treatment of HUT102 cells with 20 μM MG132, 100 nM concanamycin A, or both, for 0, 0.5, 1, and 3 h, expression levels of c-Met and c-Met phosphorylation were analyzed. The values under the bands (left) and the bar graphs (right) indicate the relative ratio of c-Met phosphorylation to c-Met (right upper), or that of c-Met to β-actin (right lower). B, Expression changes of c-Met in MT-1 and ATN-1 cells after stimulation with HGF (100 ng/mL). Expression levels of c-Met were quantified at 0, 0.25, 0.5, 1, 3, and 24 h after HGF stimulation. The values under the bands (left) and the bar graphs (right) indicate the relative ratio of c-Met to β-actin.

**Supplementary Fig. S3. Effects of JQ1 and HGF on HUT102 cell proliferation**

A, Enrichment of histone markers (H3K27Ac, H3K4me1, and H3K4me3), BRD4, and MED1 in the upstream of *HGF* gene in the monocytes and acute myeloid leukemia cells that express HGF (ChIP-Atlas data). "P" and "E" indicate promoter and enhancer regions, respectively. B, Cell growth and downstream signal changes by JQ1 treatment, with and without HGF stimulation in HUT102 cells. The viable cell number was evaluated by trypan blue staining (top). The *y*-axis

indicates the relative cell number to the untreated control (upper). The values under the bands (lower left) and the bar graph (lower right) indicate the relative ratio of phosphorylated Akt/total amount of Akt expression. Error bars indicate the standard deviation (SD). *$P < 0.05$, **$P < 0.01$.

**Supplementary Table S1. Sequences of primers and shRNA**

**Primer sequences for qRT-PCR**

| Target gene | Primer sequence (5' to 3') |
|---|---|
| *HGF* | Forward: ACTGCAGACCAATGTGCTAATAGA |
| | Reverse: TGCTATTGAAGGGGAACCAG |
| *c-Met* | Forward: TTACGGACCCAATCATGAGC |
| | Reverse: ATAAGTCAACGCGCTGCAA |
| *CCL2* | Forward: AGCAAGTGTCCCAAAGAAGC |
| | Reverse: GCTGCAGATTCTTGGGTTGT |
| *CCR2* | Forward: CTGAGACAAGCCACAAGCTG |
| | Reverse: GACTTCTTCACCGCTCTCGT |
| *GAPDH*, TaqMan | Hs00266705_g1, Thermo Fisher Scientific |

**Primer sequences for plasmid construction**

| Target gene | Primer sequence (5' to 3') |
|---|---|
| *HGF* | Forward: TTGCTACAGGCATCGTGGTGTC |
| | Reverse: GCGCCCACCCTTTCATGACTGTGGTACCTTATATGTTAAA |

**Primer sequences for ChIP-qPCR**

| Target gene | Primer sequence (5' to 3') |
|---|---|
| *HGF-E* | Forward: CAACTGCCCTTTGAGGAAAA |
| | Reverse: GAGAAGCTGCAGAACTGTTGG |
| *HGF-P* | Forward: GTGCCTAAAAGAGCCAGTCG |
| | Reverse: AGGGGGCTGGAAGAGAGTAA |

**shRNA targeting sequences**

| Target gene | Target sequence (5' to 3') |
|---|---|
| *Luciferase* | GTGCGTTGCTAGTACCAAC |
| *HGF#1* | GATTGATTTACCTAATTAT |
| *HGF#2* | GCAAAGACTACCCTAATCA |